Dalton Transactions

Accepted Manuscript

ROYAL SOCIETY OF CHEMISTRY

www.rsc.org/dalton

A first-principles investigation of oxygen reduction reaction catalysis capabilities of As decorated defect graphene

Dipayan Sen,[a] Ranjit Thapa[b] and Kalyan Kumar Chattopadhyay*[a]

Abstract

Single and multiple As adatom adsorptions on double vacancy (DV) defect graphene sheets are extensively analyzed using dispersive force corrected density functional theory (DFT). Defect pentagonal and heptagonal bridge sites and the immediate neighborhood of the defect center are found to be most favorable for this purpose. Quantitative analysis of electronic structures revealed the As-C bonding to be mostly ionic in nature with some covalency arising from the overlap of As p states and C p states. For multiple As adatoms adsorption in close vicinity, ionicity of the As-C bonds are found to decrease to support As-As cohesion; the net result of which is manifested as better binding of dioxygen molecule with them and additional weakening of the O-O bond in the adsorbed state. Free energy profile of oxygen reduction reaction (ORR) cycle using multiple As atom adsorbed DV graphene as electrocatalyst predicts high affinity towards four electron process and forbids the formation of H_2O_2 via two electron process. Other traits, such as no intermediate O-O-H formation and high stability of the catalytic system throughout the reaction process indicate As adatoms adsorbed on DV graphene system to be efficient and highly stable as an alternate Pt free ORR electrocatalyst.

Introduction

For conversion and storage of chemical energy (e.g. fuel cells)[1, 2] or renewable energy (solar cells)[3-6], Pt or Pt derived electrocatalyst materials are widely used at anodes/cathodes or counter electrodes. However, current research developments are continually proving the usage of traditional Pt based electrocatalysts to be *passé* owing to drawbacks such as inactivation of the catalytic surfaces by fuel crossover or adsorption of carbon monoxide on the active catalytic sites of H_2-O_2 fuel cells[7, 8], sub per performance while using sulfur containing redox electrolytes in case of dye-sensitized solar cells[9, 10] etc. The above, coupled with inadequacy of Pt reservoir in earth and prohibitive cost of large scale deployment of such catalysts, have recently initiated a large scale hunt for alternate electrocatalysts. Functionalized and nanocatalyst supported carbon nanostructure based Pt-free electrocatalysts are lately attracting lots of research interests due to their low cost, higher stability and durability, improved electrocatalytic activity and their being highly resistive to CO poisoning and fuel cross-over through the membrane[10-14]. Feasibility of graphene as support material for a newer generation of Pt nanoparticle based electrocatalysts is also lately being investigated in this regard[15].

Among different carbon nanostructures, graphene is particularly suitable for designing metal free electrocatalysts for oxygen reduction reaction (ORR), as 2D nature of it yields large amount of exposed surface area compared to other materials that can greatly improve catalytic performance parameter. In addition, highly active doping or adsorption sites can be engineered into graphene lattice by incorporation of defects. Till now, formation of several types of defects on graphene sheet have been theoretically calculated and experimentally observed, namely defects arising due to pure rearrangement (Stone-Wales defect)[16], or reconstruction due to removal of one[17], two[18] or multiple carbon atoms[19] from the graphenic lattice. Among them,

double vacancy (DV) defects, produced by coalescence of two single vacancies (SV) or by removing two adjacent atoms, seems most suitable for adatom or cluster adsorptions, as they are thermodynamically more favorable and practically immobile up to very high temperatures[20]. For fully reconstructed DV defects in graphene that has no dangling bonds, three separate DV configurations are possible, namely DV(5-8-5) (containing two pentagons and one octagon), DV(555-777) (containing three pentagons and three heptagons) and DV(5555-6-7777) (containing four pentagons, one rotated hexagon and four heptagons), among which the DV(555-777) configuration being energetically most stable[20]. As activation energies required for switching between different DV configurations are reported to be quite high[20], DV(555-777) defect graphene presents itself as an interesting host for adsorption related investigations.

Previous reports suggest[21-23], incorporation of Pd on pristine/ defect graphene can vastly improve ORR catalysis capabilities by facilitating better electron transfer to dioxygen molecules and weakening the O-O bonds. However, one of the major concerns stifling the practical applications of the same is: Pd adatoms on graphene surface tend to migrate and eventually form large agglomerations[24] rather than fine dispersions, and thus deteriorate the overall catalytic performance parameter. Arsenic, as an adsorbate in a similar scenario possesses greater prospective as electronegativity (χ) of As is comparable to that of Pd (indicating possibility of comparable ORR performance) while it has much lower cohesive energy[25] (indicating lesser probability of agglomeration). As adsorption on graphene and graphene derivative host systems has lately become a major focus of attention in the experimental community[26-32] from an altogether different point of view also. Arsenic is one of the most toxic ground water contaminants that is currently generating supreme health concerns over a global scale; and graphene and its derivatives show excellent promise for storage and removal for As via

adsorption in a highly efficient and cost effective manner[26-32]. Any probable approach to recycle and utilize As adsorbed graphene/ graphene derivative media which are usually obtained in the above processes for emerging environment-friendly applications such as energy storage could well prove to be invaluable. Even though the aforementioned experimental results demonstrate great promise, to the best of the authors' knowledge, till now, no extensive theoretical investigation probing the interactions of As adatom(s) with complex defect sites of graphene or the prospect of the same as ORR electrocatalyst is reported, and with the current work, the authors' aim to fill up that void.

In the current work, the authors' present an exhaustive and systematic study on single and multiple As adatom(s) adsorption on DV(555-777) defect graphene surface using dispersive force corrected density functional theory. Stabilities of different adsorption configurations are compared against each other to identify the most probable adsorption configurations. Nature of As-C interactions and the associated bonding mechanisms are thoroughly investigated by the means of rigorous electronic structure calculations. Catalytic properties of the most favorable configurations of As adsorbed on DV(555-777) defect graphene systems for cathodic oxygen reduction reaction are analyzed in detail and are compared with the same of pristine/ DV(555-777) defect graphene systems, substitutional N doped pristine graphene system and Pt(1 1 1) surface. Performance of the proposed As adsorbed on DV(555-777) defect graphene electrocatalyst in each steps of ORR cycle is also quantitatively estimated using first-principles calculation.

Theoretical methods

Our first-principles calculations were performed by Vienna *ab initio* simulation package (VASP)[33-36] using projector-augmented-wave (PAW)[37] approach to describe the ion cores. Perdew–Burke–Ernzerhof (PBE) functional[38] within the generalized gradient approximation (GGA) was used to deal with the exchange and correlation terms. Plane wave basis up to an energy cut off 520 eV were used in all calculations. For structural optimizations, Brillouin zone integrations were performed using **k**-points spacing of ~0.5/Å (actual value: 0.495×0.495×0.314 /Å) centered at the ***Γ*** point for 6×6×1 graphene supercell containing 72 C atoms (± defect atoms/ adsorbates). For all electronic properties calculations, a much finer ~0.1/Å (actual value: 0.099×0.099×0.314 /Å) **k**-point spacing was deployed. For geometrical optimization, the systems were allowed to fully relax until the forces were converged below 1×10^{-2} eV/Å. All calculations were performed in spin unrestricted manner. Bader analysis[39] was used to quantitatively analyze the charge transfer between the adatoms and hosts. Contributions of dispersive forces were taken into account to facilitate improved accuracy by using PBE+D2 forcefield (Grimme's) method[40] which as per the previous reports[41] provides one of the best balanced results.

Graphene surface was built by cleaving the geometrically optimized graphite (space group P63/mmc) structure followed by further optimization. Thus obtained graphene unit cell consisted of two carbon atoms and had lattice parameter of a = b = 2.44 Å, which is in good agreement with previously reported values[42]. A vacuum slab of length 20 Å was used in perpendicular direction to the graphene plane to ward off the spurious interactions with its own periodic image. DV(555-777) defect graphene model was built by removing two carbon atoms from a 6×6×1 supercell of graphene containing seventy two carbon atoms (resulting in defect

concentration ~ 2.7%), rotating the bonds as required and then geometrically optimizing the resulting structure.

The stability of the As adatom on the defect/pristine graphene host was determined from first principle analysis. This was done by calculating the adsorption energy of the system where more negative value of the adsorption energy signifies better stability. For the current systems, the adsorption energy can be defined as:

$$E_{ads} = E_{tot} - E_{far} \qquad (1)$$

Where, E_{ads} is the adsorption energy of the As adatom on defect/ pristine graphene system, E_{tot} is the total energy of the As adsorbed defect/ pristine graphene system and E_{far} is the total energy of defect/ pristine graphene adsorbent and As adsorbate when they are sufficiently far (~ 10 Å) *i.e.* in a non-bonding state. Dioxygen adsorption capacity of As adsorbed defect/ pristine graphene system was derived using a similar approach. The adsorption energy in this case was computed by the following relation:

$$E^{O}_{ads} = E^{O}_{tot} - E^{O}_{far} \qquad (2)$$

Where, E^{O}_{ads} is the adsorption energy of dioxygen on a host, E^{O}_{tot} is the total energy of the dioxygen adsorbed host and E^{O}_{far} is the total energy of dioxygen adsorbate and host adsorbent when they are sufficiently far (~ 10 Å) *i.e.* in a non-bonding state.

Results and discussions

Stability of As adatom(s) on double vacancy defect graphene sheet

To study As adsorption on double vacancy defect graphene sheet, as first step, As adsorption on pristine graphene sheet was investigated. There are three highly symmetric sites on pristine

graphene sheet (which has a planar hexagonal, honeycomb like crystal structure) – directly over a carbon atom *i.e.* atop site (A), over a C-C bond *i.e.* bridge site (B) and over the center of a hexagon *i.e.* middle site (M); upon which a foreign adatom could adsorb. However interactions of each of these sites with foreign adorbates are markedly different, which could be readily verified from numerous previous reports[20] on difference of adsorption energetics of various adatoms upon these sites. Our obtained results indicate, for As adatom adsorption on pristine graphene system, only B sites present a plausible choice as when As adatoms are placed on either A or M sites and relaxed, they tend to migrate to the nearest B sites. Using Eq. 1 and not considering the contribution from dispersive forces (only PBE), we obtained adsorption energy of -1.49 eV for single As adatom adsorption on the B site of a 6×6×1 supercell of pristine graphene sheet. For the same, when the contributions from Van der Waals interactions were taken into account (PBE+D2) for a more realistic description of the resultant system, we obtained slightly lower adsorption energy of -1.70 eV. The above implies that the stability of As adatom on graphene sheet is quite high (and possibly spontaneous). For stable B site adsorption of As adatom on pristine graphene sheet as described above, lengths of the two As-C bonds were calculated to be 2.12 Å each, and for the same case, each of the two nearest C atoms of As adatom were observed to lift up from the graphene plane by small distances of 0.21 Å. These local distortions of graphenic lattice near the adsorption sites illustrate strong nature of As-C bonding.

Armed with the above analysis, we consider the more complex scenario of interaction of As adatoms with double vacancy (DV) defect graphene system next. Presence of multiple pentagons and heptagons on a DV(555-777) defect graphene sheet modifies the local symmetry of graphene lattice by a great degree and introduces the possibility multiple types of A, B and M

site adsorption configurations. We use the following convention to denote and identify them: A, B and M denote atop, bridge and middle sites respectively as usual; while the numbered subscripts denotes polygons: for A site, 'common vertex of'; for B site, 'common bridge of' and for M site, 'center of'. Behavior of As adatoms on pristine graphene would imply that only the B sites of DV(555-777) is of relevance from adsorption perspective. However, as we will show, the most favorable sites for single As adatom adsorption on DV(555-777) graphene are not necessarily the B sites and they could only be identified if all possibilities are considered exhaustively and systematically. For B site adsorption of As on DV(555-777) defect graphene, the following highly symmetric configurations were considered: B_{76} (where subscript $_{76}$ denotes: As adatom adsorption on common bridge of a heptagon and a hexagon), B_{75}, B_{77}, B_{56} and B_{66} and they are schematically shown in Fig. 1 by black dots. Obtained results indicate, though relative stabilities vary, stable single As adatom adsorption is feasible for all of these five configurations; and among them, adsorption of As at B_{75} configuration is most favorable. We obtained adsorption energy of -1.83 eV using only PBE and total adsorption energy of -2.03 eV while using PBE+D2 for this case; which are significantly lower (-0.34 eV and -0.33 eV respectively) than the same for single As adatom adsorption on B sites of pristine graphene and thus indicating increased stability of As adatom for this configuration. For the same, we obtained As-C bond lengths of 2.10 Å and 2.07 Å respectively and observed the nearest two C atoms of As to rise up from the graphene plane by small distances of 0.22 Å and 0.21 Å respectively which indicates presence of strong As-C bonding in this case. For As adatom adsorption at B_{76}, B_{77}, B_{56} and B_{66} configurations, we obtained comparatively higher As adsorption energies of -1.49 eV, -1.93 eV, -1.47 eV and -1.44 eV (using PBE+D2) respectively. Notably, among all B sites, As adsorption at B_{66} configuration *i.e.* on common bridge of two hexagons is found to be

least likely energetically, generalizing the notion that defect sites of graphene in this case provides better adsorption locations to As adsorbates. Variation of As adsorption energies (corrections for dispersive forces included) across different B sites of DV(555-777) graphene is graphically shown in Fig. 1 and optimized configurations of As adsorbates on B_{76}, B_{75}, B_{77}, B_{56} and B_{66} configurations are shown in Fig. 2 (a)-(e) respectively. Value of As-C bond lengths and upshift of nearest C atoms to the As adsorbates for each cases of B site adsorptions indicate strong As-C bonding occurs for each of them. Values of As adsorption energies with and without dispersive corrections along with As-C bond lengths for stable configurations of As adatom adsorption on pristine and DV(555-777) defect graphene are listed in Table 1.

Trends of A and M site adsorptions of As adatoms on pristine graphene imply that, it is likely for various A and M sites of DV(555-777) to not provide any stable adsorption sites for As adatoms. Nevertheless, behavior As adatoms on these sites provides a convenient tool to search more extensively for additional local minima of potential energy surface if they are present. We systematically investigated behavior of As adatoms on various A and M sites of DV(555-777) defect graphene; namely at A_{777} (where subscript $_{777}$ denotes As adatom adsorption on common vertex of three heptagons), A_{757}, A_{756}, A_{566}, A_{766}, A_{666}, M_7 (where subscript $_7$ denotes As adatom adsorption on the center of a heptagon), M_5 and M_6 sites (shown schematically in Fig. 1; A sites by black star and M sites by black plus symbols). As adatoms, when relaxed on these configurations, tend to move to the nearest available stable sites, *e.g.* $A_{756} \rightarrow B_{75}$, $A_{566} \rightarrow B_{56}$, $A_{766} \rightarrow B_{76}$, $A_{666} \rightarrow B_{66}$, $M_5 \rightarrow B_{75}$, $M_6 \rightarrow B_{66}$. However, interestingly, an As adatom, when placed at A_{777}, A_{757} or M_7 configuration and relaxed, it migrates to a new configuration near the defect center and bonds to three C atoms, indicating this new configuration should have better stability than even the B_{75} configuration as the As adatom migrates to this site even though a nearby B_{75}

configuration is available. We denote this new configuration as T and optimized configuration of an As adatom adsorbed on this configuration is shown in Fig. 2 (f). We obtained adsorption energy of -1.88 eV using only PBE and -2.10 eV using PBE+D2 for this configuration, indicating the same to be most stable among all configurations for single As adatom adsorption on DV(555-777) defect graphene sheet. For T configuration, we calculated the As-C bond lengths to be 2.20 Å, 2.07 Å and 2.19 Å respectively and observed the nearest three C atoms of As to rise up from the graphene plane by small distances of 0.28 Å, 0.08 Å and 0.26 Å respectively, which implies occurrence of strong As-C binding in this case.

Thus identifying the stable configurations for single As adatom adsorption on DV(555-777) defect graphene, we analyze the possible scenarios of multiple As adatom adsorptions next. As is evident from Fig. 2(f), on DV(555-777) defect graphene, there are three symmetric T configurations per DV; however, inter-site separation between them are low (~1 Å), so it is unlikely for two As adatoms to adsorb on two T configurations of the same face of a single DV(555-777) defect site. Indeed, when two As adatoms are placed at two T configurations and relaxed, we found them to migrate far from each other to result in an unstable configuration. On the other hand, one As adatom placed at most favorable T configuration and another As adatom placed at a nearby second most favorable B_{75} configuration will seem more reasonable. However, in that case, after relaxation, both the As adatoms were found to migrate to two nearby A_{757} sites. The optimized structure of the above (we denote it by $2A_{757}$) is shown in Fig 3. (a). We calculated -3.19 eV adsorption energy/ As adatom using PBE and -3.39 eV adsorption energy/ As adatom using PBE+D2 for $2A_{757}$ configuration. To test whether multiple As adatom adsorption on adjacent sites or far sites of DV(555-777) is more likely, we compared the stability of $2A_{757}$ against a configuration in which one As adatom is adsorbed on the most stable T

configuration and another As adatom is adsorbed on a B_{66} configuration (we denote it by T-B_{66}), which provides furthest distance between the adatoms. Optimized structure of T-B_{66} configuration is shown in Fig. 3 (b) and we obtained much higher adsorption energies/ As adatom of -1.52 eV while using PBE only and -1.74 eV while using PBE+D2 for this case. Similar comparisons between various two As adatom adsorption configurations on DV(555-777) defect graphene sheet revealed $2A_{757}$ to be most favorable. An analogue of the above study was also performed for three As adatoms adsorption on DV(555-777) defect graphene; and similar to the above, three As adatom adsorptions on three A_{757} sites of DV(555-777) defect graphene (we denote it by $3A_{757}$) as shown in Fig. 3 (c) was found to be most favorable with adsorption energies/ As adatom of -3.66 eV using only PBE and using -3.85 eV using PBE+D2. In comparison to $2A_{757}$, for $3A_{757}$ configuration, the As-C bond lengths were found to increase by 0.45 Å ~ 0.54 Å and also the average upshift of nearest C atoms to the As adatoms were observed to decrease (as evident from close up side views of $2A_{757}$ and $3A_{757}$ as shown in Fig. 3 (d) and (e) respectively) by 0.16 Å. Observed improved stability for $3A_{757}$ configuration in spite of As-C bond lengthening could be explained by cohesion of As atoms decreasing the ionicity of As-C bonds at the cost of contributing to the net stability of the resultant system. A validation of the above hypothesis can readily be obtained by quantitatively estimating the amount of As-As cohesion present in $2A_{757}$ and $3A_{757}$ configurations while constraining the As adatoms in their adsorption geometries sans the substrate. Cohesive energy of bulk As is 2.96 eV/ atom[25] and in comparison to that, we obtained cohesive energies of 1.99 eV/ atom and 2.17 eV/atom for As adatoms in $2A_{757}$ and $3A_{757}$ geometries respectively (while keeping the substrate interactions decoupled) which quantifies the increase of As-As cohesion in case of $3A_{757}$ configuration. Values of As adsorption energies using PBE and PBE+D2 and corresponding As-C bond lengths

for stable configurations of multiple As adatom adsorption on DV(555-777) defect graphene are listed in Table 1. The above study demonstrates that in case of multiple As adatom adsorption on DV(555-777), adsorptions at adjacent sites are more likely and in a practical scenario, DV defects can act as seeding center for As clusters.

Electronic Properties

To investigate the strong nature of As-C bonding as demonstrated above, the electronic properties of As adatom(s) adsorption on DV(555-777) defect graphene are investigated next. Total density of states (TDOS) graph of DV(555-777) defect graphene, as used in our calculations, is shown in Fig. 4 (a). Previous works[43] reported 0.3 eV calculated band gap for DV(5555-6-7777) defect graphene but no band gap for DV(555-777) defect graphene using systems having ~ 1% defect concentrations. Our obtained results show that the DV(555-777) defect graphene sheet, as used in our calculation have a small energy gap of ~ 0.1 eV near Fermi level. As the defect concentration is nearly thrice for the current case (2.7%), it can be concluded that, for higher defect concentration, a small gap opening occurs whose value decreases with the decrease of defect concentration and tends to that of the pristine graphene for the limiting case. Adsorption of As adatom significantly modifies the TDOS of DV(555-777) defect graphene and changes the nature of As adsorbed defect graphene system to metallic. The above could be confirmed from TDOS of B_{75} and T configuration which are shown in Fig. 4 (b) and (c) respectively. B_{75} configuration is found to favor a spin-polarized ground state (as evident from the asymmetry of its TDOS near Fermi level) with 9.90% spin-polarization (defined as: $100 \times ((D(E_F,\uparrow) \sim D(E_F,\downarrow)) / (D(E_F,\uparrow) + D(E_F,\downarrow)))$, where $D(E_F,\uparrow)$ and $D(E_F,\downarrow)$ represent the values of TDOS of majority spin and minority spin respectively) at the Fermi level. As p states and C p states are found to be the primary contributors to the TDOS near Fermi level for both B_{75} and T

configurations. Partial density of states (PDOS) for adsorbed As adatom's p and d orbitals and its nearest C atoms' p orbitals for B_{75} configuration are shown in Fig. 4 (d), which shows asymmetricity of the TDOS of the same near Fermi level mainly arises from As p states with minor contributions from C p states (magnified in inset, Fig. 4 (d)) and some amount of orbital overlap between the two *i.e.* hybridizations are also noticeable around Fermi level. Bonding of As adatom at T configuration is somewhat more intricate. Calculated PDOS of p and d orbitals of As adatom adsorbed on T configuration, overlaid with the cumulative PDOS of p orbitals of the three nearest C atoms are shown in Fig. 4 (e). The above confirms major contributions of As p states and minor contributions from C p states for this configuration near Fermi level. No spin polarization is observed in this case; however, around Fermi level, certain amount of orbital overlap between As p states and C p states (magnified in inset i, Fig. 4 (e)) can be observed. As shown in Fig. 2 (f), at T configuration, As adatom interacts with three C atoms, two of which are at the common vertices of two heptagons and one pentagon (we denote it by C_{757}) and the remaining one is at the common vertex of three heptagons (we denote it by C_{777}). As-C bond lengths for these two cases differ by ~ 0.2 Å ($d_{As\text{-}C}$ is lower for As-C_{777}, shown in Table 1) and subsequently the As-C_{757} and As-C_{777} interactions also differ slightly in nature. For T configuration, contribution of C_{777} p states near the immediate vicinity of the Fermi level are found to be higher than that of either of the C_{757} atoms' p orbitals (inset ii, Fig. 4 (e)), which indicates bonding due to orbital overlap is slightly stronger for As-C_{777} bond than As-C_{757} bonds. TDOS of most favorable configuration of two and three As adatom adsorption on DV(555-777) defect graphene sheet, *i.e.* $2A_{757}$ and $3A_{757}$ configurations are shown in Fig. 4 (f) i and ii respectively; which show presence of no spin-polarization. Also similar to the cases of single As adatom adsorption on DV(555-777) graphene sheet, for these cases also, the TDOS is found to

be metallic in nature with major contributions from As p orbitals and minor contributions from C p orbitals.

To gauze the ionic contribution to the As-C bonding, Bader analysis of valence charge of the relevant systems were performed. For all the cases of As adsorbed DV(555-777) defect graphene, electron transfer from adsorbate As to adsorbent defect graphene system is observed which can be readily explained by higher χ of C atoms (χ_C = 2.55) than As atoms (χ_{As} = 2.18). Consequently, the As adatoms are found to gain positive charge and its nearest C atoms are found to gain negative charge, rendering certain amount of ionicity to the As-C bonds. For B_{75} and T configurations, 0.3 e and 0.4 e positive charge transfer to the As adatom are calculated respectively, where the higher value of the later explains the improved stability of T configuration. Among all the B site adsorptions, minimum charge transfer (0.2 e to the As adatom) is obtained for B_{56} and B_{66} configuration. The above, in conjunction with the overlapping of the C p and As p orbitals as demonstrated in the DOS analysis, confirms the As-C bonding to be of mixed ionic and covalent nature. Also, for $3A_{757}$ configuration, charge transfer is found to be less (*i.e.* less ionicity of As-C bonds) than the other configurations, explaining the observed increase of As-C bond lengths in this case. Charge transfer to the As adatoms and its nearest C atoms for all the cases under consideration is listed in Table 1. Top view of deformation charge density (*i.e.* the difference charge density between the self-consistent total valence charge density and the total valence charge density obtained from superposition of total atomic charge densities placed at their lattice positions.) isosurfaces for isovalues 0.01 e/ $Å^3$ (red) and -0.01 e/ $Å^3$ (blue) for B_{75}, T, $2A_{757}$ and $3A_{757}$ configuration are shown in Fig. 5 (a)-(d) respectively which graphically illustrates the charge transfer processes.

Oxygen reduction reaction (ORR) catalysis capabilities

In the next section, feasibility of As decorated DV(555-777) graphene for ORR catalysis is computationally explored and compared with that of pristine/ DV(555-777) defect graphene, substitutional N doped pristine graphene and Pt(1 1 1) surface. To facilitate ORR at cathode, proper adsorption of O_2 is of paramount importance in the entire reaction process. For dioxygen adsorption at pristine graphene surface, in agreement with previous reports[44], we found dioxygen molecule adsorption parallel to the graphene sheet and near the center of the hexagons (top and side views are shown in Fig. 6 (a)) is most favorable. Following Eq. 2, we obtained adsorption energies of -0.16 eV using PBE and -0.32 eV using PBE+D2 for this configuration which is comparable with the -0.13 eV adsorption energy value reported by Yan et al[44] using PW91 (without considering the dispersive forces' contribution). For an isolated O_2, we calculated the O-O bond length to be 1.23 Å, which is in well agreement to the previous studies[45], however upon adsorption on the pristine graphene, the O-O bond length of the dioxygen stretches to 1.27 Å (3.25%) and charge transfers of -0.2 e to each of the O atoms are observed from Bader charge analysis. In case of DV(555-777) defect graphene, presence of multiple pentagons and heptagons gives rise to the possibility of many different symmetric sites for dioxygen molecule adsorption, among which, adsorption near defect center at A_{757}-A_{777} configuration *i.e.* directly above a B_{77} bridge (top and side views are shown in Fig. 6 (b)) is found to be most favorable having adsorption energies of -0.28 eV using PBE only and -0.43 eV using PBE+D2. In this case the O-O bond length is also found to stretch to 1.27 Å (3.25%) and for the same, charge transfers of -0.2 e also to each of the O atoms are calculated from Bader charge analysis. Values of dioxgen molecule adsorption energies with and without corrections for dispersive forces, values and stretching amount of O-O bonds upon adsorption, bond lengths of dioxygen-host bonds and

values of charge transfers to the O atoms of the dioxygen molecule for all the systems under investigation are listed in Table 2. The above shows that, presence of defect in graphene can provide marginally better bonding with O_2, however, using defect graphene alone as dioxgen adsorption media, superior ORR catalysis performance than commercially used Pt(1 1 1) or N doped pristine graphene could not be achieved, as for them ~1 eV and -1.26 eV O_2 adsorption energies are reported in the previous works[46].

As decoration on DV(555-777) defect graphene can deliver a significant thrust to its ORR catalysis performance as χ_{As} is lower than $\chi_{C,}$ and as a direct consequence of the same, better electron transfer to dioxygen from host and hence better stability of dioxygen molecules is facilitated. However, multiple As adatom adsorbed DV(555-777) graphene systems are better suited to this end than single As adatom adsorbed DV(555-777) graphene systems, as in case of the former, cohesion of As atoms decreases ionicity of As-C bonds and makes additional electron densities available for further As-O interactions. Consequently, as we will show below, multiple As adsorbed defect graphene systems demonstrate excellent dioxygen adsorption capabilities. Top and side views of optimized configurations of dioxygen molecule adsorption on the As decorated DV(555-777) defect graphene system having best adsorption energy per As adatom, *i.e.* on $3A_{757}$ configuration is shown in Fig. 6 (c). For this O_2-$3A_{757}$ configuration, adsorption energies of -1.31 eV with PBE only and -1.34 eV with PBE+D2 are obtained, which demonstrates much stronger binding of dioxygen in this case than with pristine graphene, DV(555-777) defect graphene, commercially used Pt(1 1 1) surface or previously reported N doped pristine graphene systems. Also in this case, much higher stretching of O-O bonds (19.51%) and much higher amount of charge transfer to the O atoms (-0.4 e and -0.5 e) than O_2 – pristine/ DV(555-777) defect graphene are observed. Calculated high stretching of O-O bond for

O_2-3A_{757} configurations indicate O-O bond of dioxygen becomes weaker after adsorption[47]. This O-O bond weakening i.e. lowering of bond breakage barrier is highly convenient from the point of view of ORR process. However while comparing the adsorption energies, it should be noted that previous computations[46] were mostly performed using PW91 and without taking contribution for the dispersive forces into account. Also, using PBE, Lim et al[15] obtained even higher O_2 adsorption energies on Pt nanoparticles supported on defective graphene systems than the current case. For theoretically evaluating the efficiency of a prospective ORR electrocatalyst, favorable values of O_2 adsorption energy is merely a primary indicator and for a robust prediction, several other factors such as nature of free energy profile for each steps of the reaction process and possibility of H_2O_2 evolution etc. must be taken into account.

Equipped with the above analysis, the changes of free energy ($\Delta G = \Delta E - T\Delta S$, ΔE represents the change in enthalpy (here binding energy of the molecules) and ΔS is the change in the entropy) during each steps of the protonation process, as would occur in a low temperature acidic media based fuel cell (LTFC; a standard H_2-O_2 fuel cell) while utilizing an As decorated defect graphene as electrocatalyst is investigated next. In this process, the suggestion put forward by Nørskov et al.[48] *i.e* during the reaction $H^+ + e = \rightarrow \frac{1}{2}H_2$ in standard condition both the reactant and the product remain in equilibrium, is followed. The entropy changes were obtained from a physical chemistry table, assuming H_2 and O_2 gases are at room temperature and ambient pressure[49]. At ambient condition The following TS values were used: for H_2 0.41 eV, for O_2 0.64 eV and for H_2O 0.67 eV. Entropy of the adsorbed molecules was accounted for as negligible in comparison to the gas phases. Each steps of the free energy change was calculated using the above protocol. Energy of water molecules in gas phase were considered as reference energy for plotting a free energy change vs reaction step graph. Step by step changes of the free energy

during the four electron oxygen reduction reaction are shown graphically in Fig. 7 and optimized structures calculated in various steps of the simulated ORR process are illustrated in the insets of Fig. 7. In the step 1, the O_2 molecule is far from the surface and the four protons flow through the electrolyte and the four electrons travel through the outer circuit. Dioxygen molecule adsorption on catalytic surface of $3A_{757}$ configuration is shown in step 2. The adsorbed dioxygen molecule in this case is more active than free O_2 molecules owing to the lowering of bond breakage barrier as described in the last section. During the first protonation, the O-O bond breaking occurs, resulting in a single -OH radical and a single O atom adsorbed $3A_{757}$ as an intermediate step, which is shown in step 3. Notably, optimized structures of this step clearly indicates that the formation of O-O-H and consequently the formation of H_2O_2 (byproduct two electron process) is highly unlikely for the catalytic system under investigation. As a result, the efficiency and durability of the catalyst support can be vastly improved when using the proposed As-defect graphene electrocatalyst. In the step 4, formation of two -OH radical adsorbed $3A_{757}$ catalytic surface during second protonation is illustrated. Configuration of the optimized structure convey that the OH molecule on the surface are stable enough to limit desorption of -OH in the electrolyte. In the step 5 and 6, subsequent desorption of one and two H_2O molecules respectively from the catalytic surface via addition of two hydrogen atom ($H^+ + e^-$) are demonstrated by their optimized structures. As demonstrated in the free energy diagram, for the entirety of the reaction process, all intermediate steps are found to be monotonically exothermic in nature which implies that the occurrence of four electron ORR (which is highly desirable for LTFCs) for As – defect graphene electrocatalytic system is highly favorable. From the optimized structure of step 6, it is evident that the As - defect graphene electrocatalysts, as considered in the

current study, are highly stable, and are prepared to assist the next ORR cycle as soon as H_2O desorption of the previous cycle is finished.

Conclusions

To summarize, dispersive force corrected density functional theory is used to study the interactions between single/ multiple As adatoms and pristine/ DV(555-777) defect graphene. Extensive searches revealed the vicinity of the DV(555-777) defect center (T) to be most suitable for single As adsorption purpose. For two and three As adatom adsorptions, atop the carbon atoms at the common vertices of two heptagons and a pentagon near defect center ($2A_{757}$ and $3A_{757}$) are found to be most favorable. As-C interactions are found to be mostly ionic in nature with some amount of covalency arising from overlap of As p states and C p states. Also, while As adatom adsorption on common bridge of a heptagon and a pentagon (B_{75}) is found to favor a spin polarized ground state, all other configurations are found to favor non spin-polarized ground states.

As electronegativity (χ) of As is lower than that of C, incorporation of As adatom is found to positively influence the dioxygen molecule adsorption capacity of pristine/ DV(555-777) defect graphene host by facilitating better electron transfer to the dioxygen molecule. Multiple As adatom adsorbed DV(555-777) structures are found to be particularly well suited for this purpose, as Bader charge analysis indicated decrease in ionicity of the As-C bonds for them due to As-As cohesion being favored, which makes extra electron densities available for further bonding. Consequently, the $3A_{757}$ configuration not only showed vastly improved dioxygen adsorption capacity (-1.340 eV using PBE+D2) than pristine/ DV(555-777) defect graphene

systems, but also better performance in this regard than Pt (1 1 1) surface or N doped pristine graphene systems. High stretching of O-O bonds (19.854%), facilitated by high amount of charge transfer to the O atoms (-0.445 e and -0.505 e) is observed for O_2-3A_{757} configuration which indicates its suitability for ORR applications as in this case O-O bond breakage barrier becomes considerably lowered. Investigation of change in free energy during ORR cycle using three As adatom decorated DV(555-777) defect graphene as electrocatalyst revealed monotonically exothermic nature at each steps and strong inclination towards four electron ORR process. Formation of H_2O in lieu of H_2O_2 at the end of each ORR cycle and stability of the electrocatalyst for the entirety of the reaction was also confirmed from the optimized geometries of the intermediate reaction steps which highlight the As decorated defect graphene systems' suitability as alternate electrocatalyst for ORR in a practical scenario.

Acknowledgements

DS wishes to thank the West Bengal State Govt. for providing financial support during the execution of this work. RT wishes to thank Science and Engineering Research Board (SERB) for financial support (Grant no: SB/FTP/PS028/2013). The authors also wish to thank the University grants Commission, the Govt. of India for financial support under the 'University with potential for excellence (UPE-II)' scheme and also from TEQIP programme.

Notes and references

[a)]Thin Film and NanoScience Laboratory, Department of Physics,
Jadavpur University, Kolkata 700032, India
[b)] SRM Research Institute, SRM University, Kattankulathur 603 203
Chennai, Tamil Nadu, India
[*)] Corresponding author; email: kkc@phys.jdvu.ac.in; Phone: +913324572876

DS and RT have equal contribution to this work

1. Y. J. Wang, D. P. Wilkinson and J. Zhang, *Dalton transactions*, 2012, 41, 1187-1194.
2. F. Ye, H. Liu, W. Hu, J. Zhong, Y. Chen, H. Cao and J. Yang, *Dalton transactions*, 2012, 41, 2898-2903.
3. M. Bhagavathi Achari, V. Elumalai, N. Vlachopoulos, M. Safdari, J. Gao, J. M. Gardner and L. Kloo, *Physical chemistry chemical physics : PCCP*, 2013, 15, 17419-17425.
4. V. Johansson, L. Ellis-Gibbings, T. Clarke, M. Gorlov, G. G. Andersson and L. Kloo, *Physical chemistry chemical physics : PCCP*, 2014, 16, 711-718.
5. Z. Yu, H. M. Najafabadi, Y. Xu, K. Nonomura, L. Sun and L. Kloo, *Dalton transactions*, 2011, 40, 8361-8366.
6. Z. Yu, N. Vlachopoulos, A. Hagfeldt and L. Kloo, *RSC Advances*, 2013, 3, 1896-1901.
7. S. D. Davidson, H. Zhang, J. Sun and Y. Wang, *Dalton transactions*, 2014, DOI: 10.1039/c4dt00521j.
8. N. Daems, X. Sheng, I. F. J. Vankelecom and P. P. Pescarmona, *Journal of Materials Chemistry A*, 2014, 2, 4085-4110.
9. Z. Yu, H. Tian, E. Gabrielsson, G. Boschloo, M. Gorlov, L. Sun and L. Kloo, *RSC Advances*, 2012, 2, 1083-1087.

10. J. D. Roy-Mayhew, G. Boschloo, A. Hagfeldt and I. A. Aksay, *ACS applied materials & interfaces*, 2012, 4, 2794-2800.

11. Y. Wang, X. Cui, L. Chen, C. Wei, F. Cui, H. Yao, J. Shi and Y. Li, *Dalton transactions*, 2014, 43, 4163-4168.

12. X. Liu, K. X. Yao, C. Meng and Y. Han, *Dalton transactions*, 2012, 41, 1289-1296.

13. R. Li, Z. Wei, X. Gou and W. Xu, *RSC Advances*, 2013, 3, 9978-9984.

14. L. Chen, X. Cui, Y. Wang, M. Wang, R. Qiu, Z. Shu, L. Zhang, Z. Hua, F. Cui, C. Wei and J. Shi, *Dalton transactions*, 2014, 43, 3420-3423.

15. D.-H. Lim and J. Wilcox, *The Journal of Physical Chemistry C*, 2011, 115, 22742-22747.

16. A. J. Stone and D. J. Wales, *Chemical Physics Letters*, 1986, 128, 501-503.

17. J. C. Meyer, C. Kisielowski, R. Erni, M. D. Rossell, M. F. Crommie and A. Zettl, *Nano Letters*, 2008, 8, 3582-3586.

18. D. Sen, R. Thapa and K. K. Chattopadhyay, *International Journal of Hydrogen Energy*, 2013, 38, 3041-3049.

19. B. W. Jeong, J. Ihm and G.-D. Lee, *Physical Review B*, 2008, 78, 165403.

20. F. Banhart, J. Kotakoski and A. V. Krasheninnikov, *ACS Nano*, 2010, 5, 26-41.

21. M. H. Seo, S. M. Choi, H. J. Kim and W. B. Kim, *Electrochemistry Communications*, 2011, 13, 182-185.

22. X. Liu, C. Meng and Y. Han, *The Journal of Physical Chemistry C*, 2013, 117, 1350-1357.

23. T.-T. Jia, C.-H. Lu, K.-N. Ding, Y.-F. Zhang and W.-K. Chen, *Computational and Theoretical Chemistry*, 2013, 1020, 91-99.

24. I. Cabria, M. Lopez and J. Alonso, *Physical Review B*, 2010, 81, 035403.

25. C. Kittel and P. McEuen, *Introduction to solid state physics*, Wiley, New York, 8th edn., 1986, pp. 50.

26. V. Chandra, J. Park, Y. Chun, J. W. Lee, I.-C. Hwang and K. S. Kim, *ACS Nano*, 2010, 4, 3979-3986.

27. A. K. Mishra and S. Ramaprabhu, *Desalination*, 2011, 282, 39-45.

28. X.-L. Wu, L. Wang, C.-L. Chen, A.-W. Xu and X.-K. Wang, *Journal of Materials Chemistry*, 2011, 21, 17353-17359.

29. J. Zhu, R. Sadu, S. Wei, D. H. Chen, N. Haldolaarachchige, Z. Luo, J. A. Gomes, D. P. Young and Z. Guo, *ECS Journal of Solid State Science and Technology*, 2012, 1, M1-M5.

30. K. Zhang, V. Dwivedi, C. Chi and J. Wu, *Journal of hazardous materials*, 2010, 182, 162-168.

31. L. Li, G. Zhou, Z. Weng, X.-Y. Shan, F. Li and H.-M. Cheng, *Carbon*, 2014, 67, 500-507.

32. S. Vadahanambi, S. H. Lee, W. J. Kim and I. K. Oh, *Environmental science & technology*, 2013, 47, 10510-10517.

33. G. Kresse and J. Hafner, *Physical Review B*, 1993, 47, 558-561.

34. G. Kresse and J. Hafner, *Physical Review B*, 1994, 49, 14251-14269.

35. G. Kresse and J. Furthmüller, *Computational Materials Science*, 1996, 6, 15-50.

36. G. Kresse and J. Furthmüller, *Physical Review B*, 1996, 54, 11169-11186.

37. P. E. Blöchl, *Physical Review B*, 1994, 50, 17953-17979.

38. J. P. Perdew, K. Burke and M. Ernzerhof, *Physical Review Letters*, 1996, 77, 3865-3868.

39. R. F. W. Bader, *Chemical Reviews*, 1991, 91, 893-928.

40. S. Grimme, *Journal of Computational Chemistry*, 2006, 27, 1787-1799.

41. P. Janthon, F. Vines, S. M. Kozlov, J. Limtrakul and F. Illas, *The Journal of chemical physics*, 2013, 138, 244701.

42. G. Giovannetti, P. A. Khomyakov, G. Brocks, V. M. Karpan, J. van den Brink and P. J. Kelly, *Physical Review Letters*, 2008, 101, 026803.

43. A. V. Krasheninnikov and R. M. Nieminen, *Theor Chem Acc*, 2011, 129, 625-630.

44. H. J. Yan, B. Xu, S. Q. Shi and C. Y. Ouyang, *Journal of Applied Physics*, 2012, 112, 104316.

45. D. A. Outka, J. Stöhr, W. Jark, P. Stevens, J. Solomon and R. J. Madix, *Physical Review B*, 1987, 35, 4119-4122.

46. Y. Feng, F. Li, Z. Hu, X. Luo, L. Zhang, X.-F. Zhou, H.-T. Wang, J.-J. Xu and E. G. Wang, *Physical Review B*, 2012, 85, 155454.

47. K. Gong, F. Du, Z. Xia, M. Durstock and L. Dai, *Science*, 2009, 323, 760-764.

48. J. K. Nørskov, J. Rossmeisl, A. Logadottir, L. Lindqvist, J. R. Kitchin, T. Bligaard and H. Jónsson, *The Journal of Physical Chemistry B*, 2004, 108, 17886-17892.

49. A. B. Anderson, R. A. Sidik, J. Narayanasamy and P. Shiller, *The Journal of Physical Chemistry B*, 2003, 107, 4618-4623.

Configuration	$E^{(PBE)}_{ads}$ / Adatom (eV)	$E^{(PBE+D2)}_{ads}$ / Adatom (eV)	d_{As-C} (Å)	Q_{As} (e)	Q_C (e)
As - Pristine Graphene	-1.49	-1.70	2.12, 2.12	0.2	-0.1, -0.2
B_{76}	-1.27	-1.49	2.12, 2.11	0.3	-0.2, -0.1
B_{75}	-1.83	-2.03	2.10, 2.07	0.3	-0.2, -0.2
B_{77}	-1.73	-1.93	2.08, 2.08	0.3	-0.2, -0.1
B_{56}	-1.28	-1.47	2.13, 2.13	0.2	-0.2, -0.1
B_{66}	-1.23	-1.44	2.11, 2.12	0.2	-0.1, -0.2
T	-1.88	-2.10	2.20 (As-C_{757}), 2.07 (As-C_{777}), 2.19 (As-C_{757})	0.4	-0.1 (As-C_{757}), -0.1 (As-C_{777}), -0.1 (As-C_{757})
$2A_{757}$	-3.19	-3.39	2.21, 2.21	0.2,0.2	-0.1, -0.1
T-B_{66}	-1.52	-1.74	T: 2.19 (As-C_{757}), 2.05 (As- C_{777}), 2.22 (As-C_{757}); B_{66}: 2.12, 2.13	T: 0.4, B_{66}: 0.2	T: -0.1 (C_{757}), -0.1 (C_{777}), -0.1 (C_{757}); B_{66}: -0.1, -0.1
$3A_{757}$	-3.66	-3.85	2.70, 2.66, 2.75	0.1, 0.1, 0.1	0, -0.1, -0.1

Table 1: Parameters of single and multiple As adatom(s) adsorption on pristine/ DV(555-777) defect graphene systems: $E^{(PBE)}_{ads}$ is As adsorption energy using PBE only, $E^{(PBE+D2)}_{ads}$ is As adsorption energy using PBE+D2, d_{As-C} is the optimized bond length between As and C atoms, Q_{As} and Q_C are the Bader charge transfers to As and C atoms respectively.

Configuration	$E^{O(PBE)}_{ads}$ / Adatom (eV)	$E^{O(PBE+D2)}_{ads}$ / Adatom (eV)	d_{O-O} (Å)	Δd_{O-O} (%)	$d_{O2-host}$ (Å)	Q_O (e)
O_2 - Pristine Graphene	-0.16	-0.32	1.27	3.25	1: 2.53, 2.54 2: 2.54, 2.53	-0.2, -0.2
O_2 - DV(555-777) (A_{757}-A_{777}; above B77)	-0.28	-0.43	1.27	3.25	2.13, 2.73	-0.2, -0.2
O_2 - $3A_{757}$	-1.31	-1.34	1.47	19.52	1.89, 1.89	-0.4, -0.5

Table 2: Parameters of O_2 adsorption on pristine/ DV(555-777) defect graphene/ As decorated DV(555-777) defect graphene hosts: $E^{O(PBE)}_{ads}$ is dioxygen adsorption energy using PBE only, $E^{O(PBE+D2)}_{ads}$ is dioxygen adsorption energy using PBE+D2, d_{O-O} is the bond length of the dioxygen, Δd_{O-O} is the amount of O-O bond stretching occurred after adsorption, $d_{O2-host}$ is the bond length between dioxygen and host system and Q_O is the Bader charge transfer to the O atoms of the adsorbed dioxygen molecule.

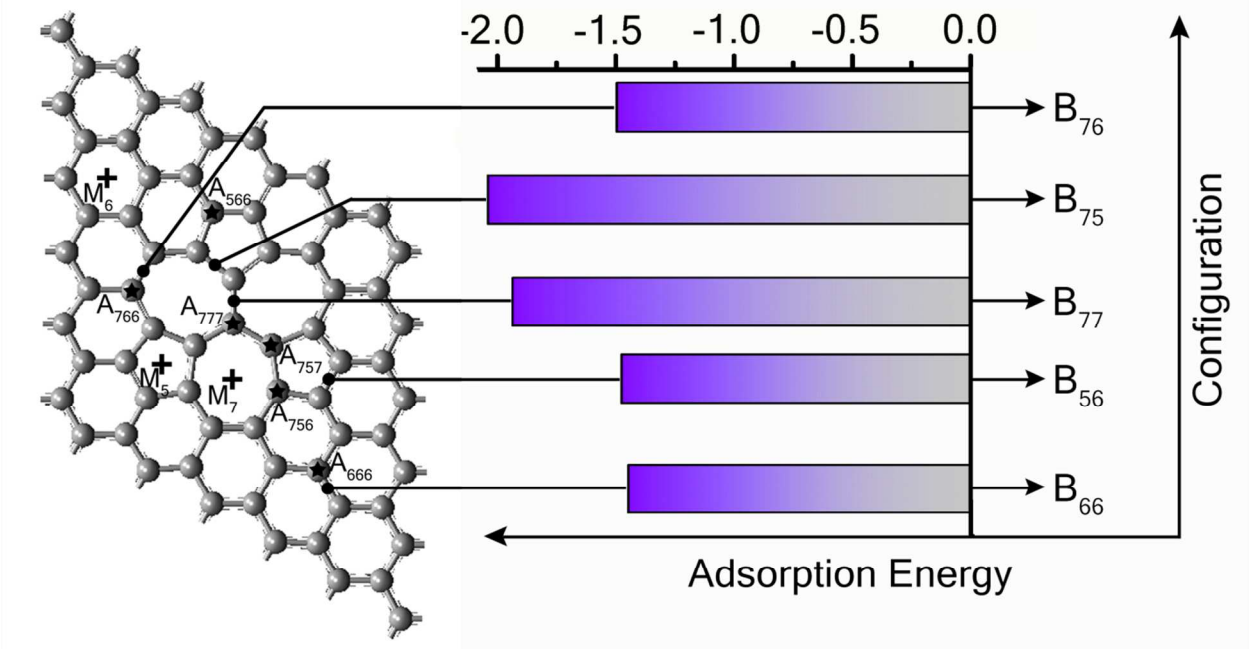

Fig. 1: Schematic representation of the most symmetric adsorption sites on DV(555-777) graphene system: A, B and M denote atop, bridge and middle sites (Exact positions of them are shown by star, dot and plus symbols respectively). The bar chart shows variation of single As adatom adsorption energies at different B sites.

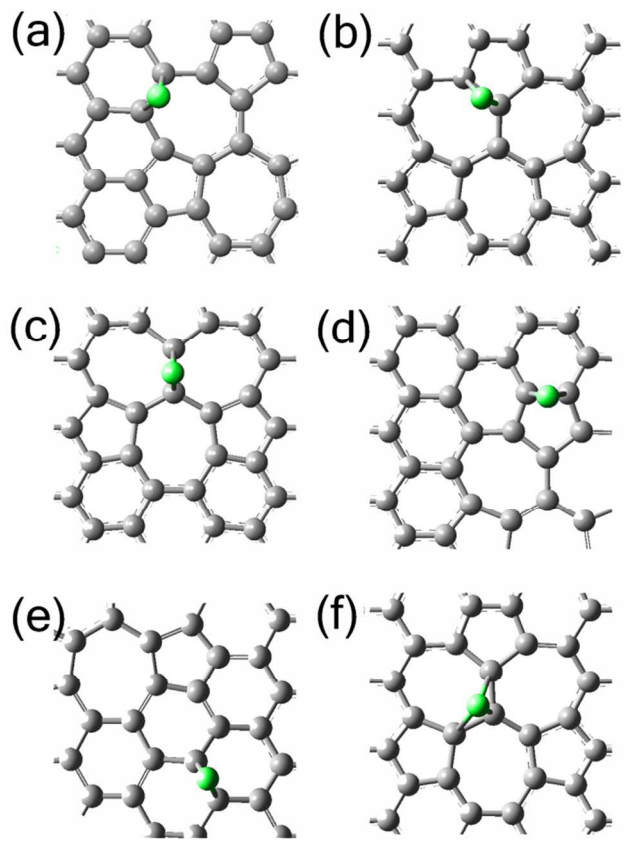

Fig. 2: Optimized structures of single As adatom adsorption on DV(555-777) defect graphene system: (a) B_{76}, (b) B_{75}, (c) B_{77}, (d) B_{56}, (e) B_{66} and (f) T

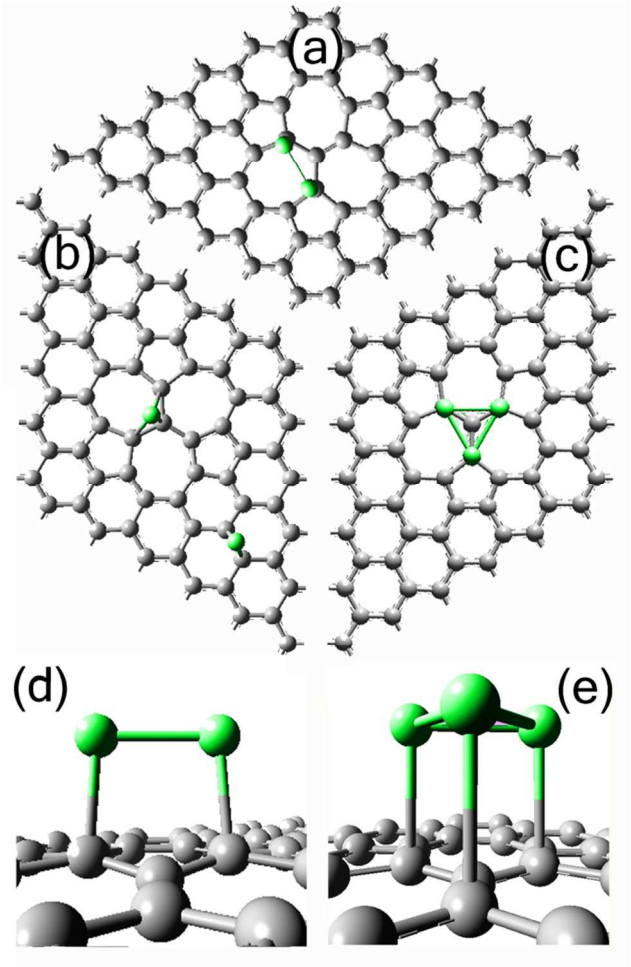

Fig. 3: Optimized structures of multiple As adatoms adsorption on DV(555-777) defect graphene system: (a) $2A_{757}$, (b) T-B_{66}, (c) $3A_{757}$, (d) and (e) close up side views of $2A_{757}$ and $3A_{757}$ configurations respectively.

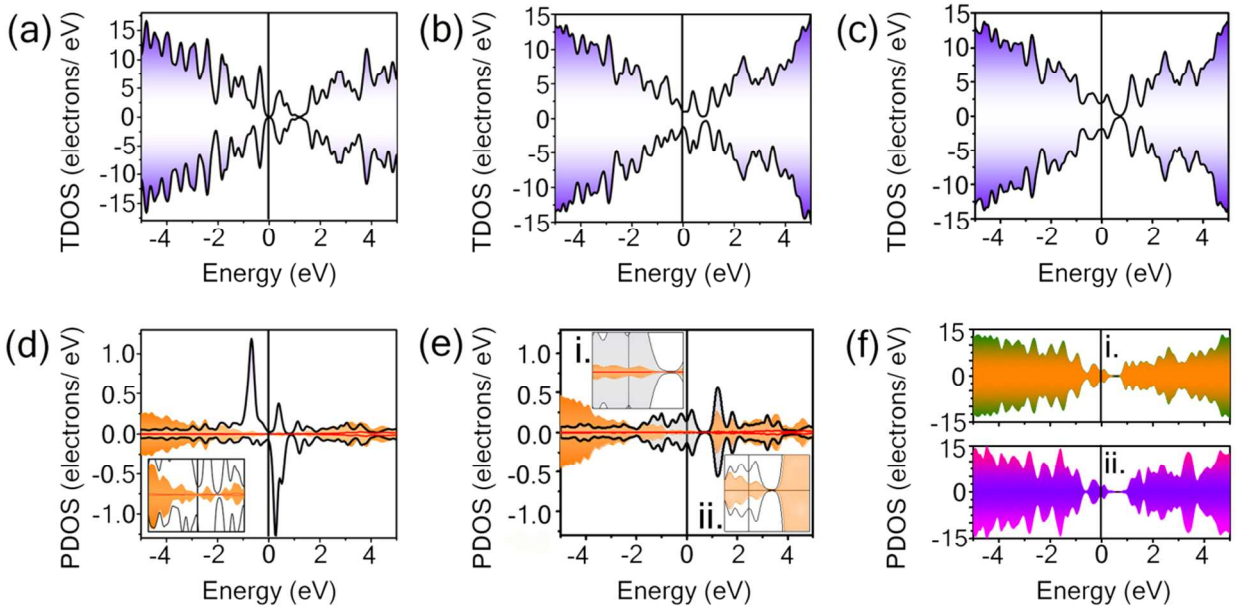

Fig. 4: Comparison of density of states (DOS): (a), (b) and (c) TDOS of DV(555-777) defect graphene, B_{75} and T configuration respectively. (d) PDOS of C p states (shaded) along with As p (black line) and d (red line) states for B_{75} configuration. Contributions from C p states near Fermi level are magnified in inset. (e) PDOS of C p states (shaded) along with As p (black line) and d (red line) states for T configuration. Cumulative contributions from C p states near Fermi level are magnified in inset (i). Inset (ii) shows relative contributions of C_{777} (black line) and C_{757} p states (shaded) near Fermi level. (f) TDOS of (i) $2A_{757}$ (ii) $3A_{757}$ configuration.

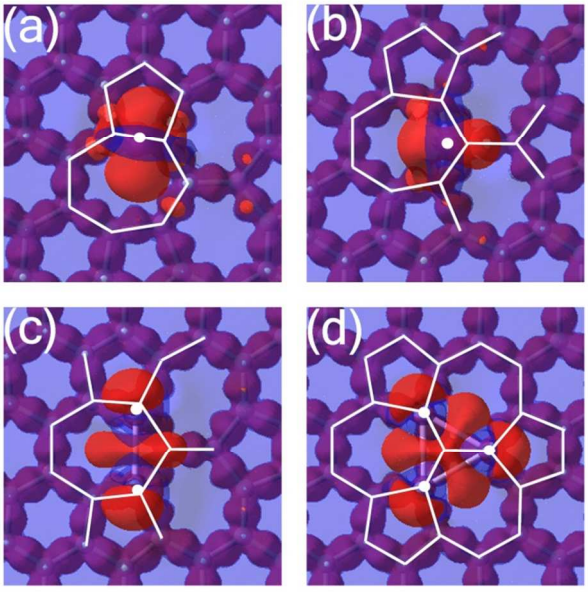

Fig. 5: Top view of deformation charge density isosurfaces (isovalues: 0.01 e/ $Å^3$ (red) and -0.01 e/ $Å^3$ (blue)) for (a) B_{75}, (b) T, (c) $2A_{757}$ and (d) $3A_{757}$ configurations.

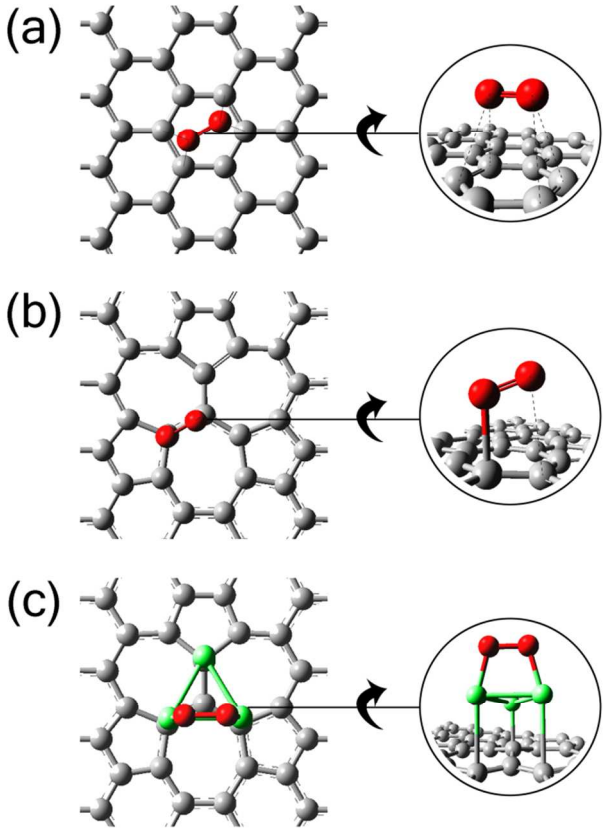

Fig. 6: Optimized configurations for dioxygen adsorption: (a) O_2 - Pristine Graphene (b) O_2 - DV(555-777) (configuration: A_{757}-A_{777}; (above B_{77})) (c) O_2 - $3A_{757}$

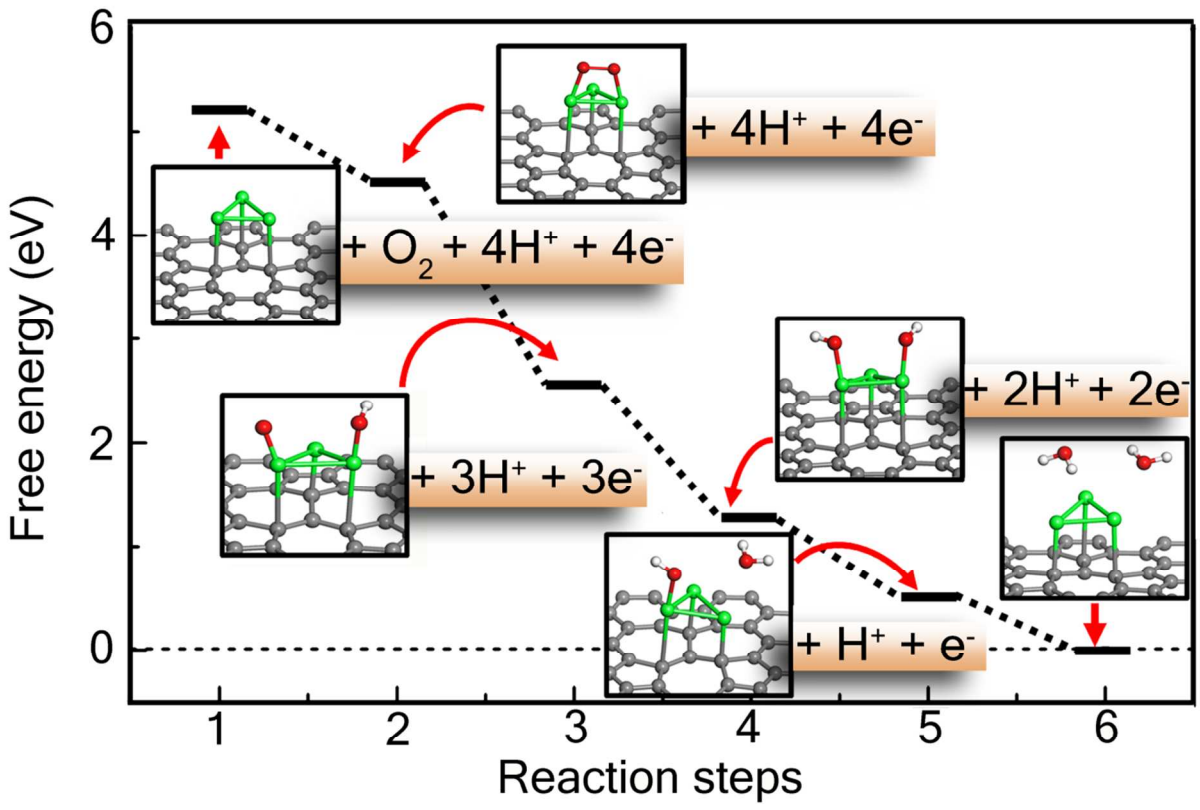

Fig. 7: Changes of free energy during oxygen reduction reaction while using As decorated DV(555-777) defect graphene as electrocatalyst. Optimized structures of the reactants during intermediate steps are shown in insets.

Table of contents entry:

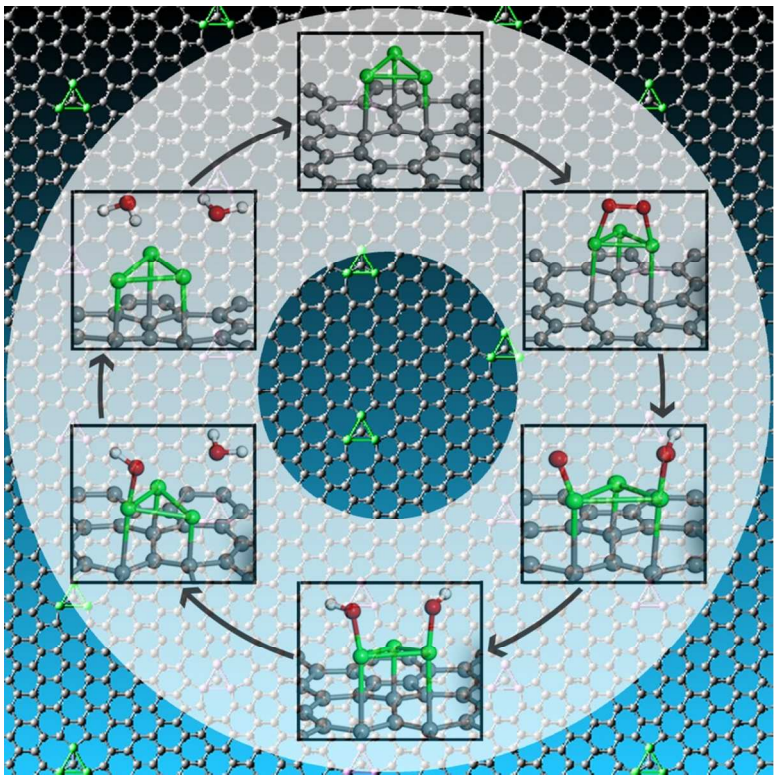

Arsenic adsorbed double vacancy defect graphene systems are found to demonstrate excellent electrocatalytic properties for oxygen reduction reaction via high affinity towards four electron process.